ECS Transactions, 35 (1) 1601-1609 (2011)
10.1149/1.3570146 ©The Electrochemical Society

Ceramic Oxide Anode with Precipitated Catalytic Nanoparticles for Ethanol Fueled SOFC

N. K. Monteiro, S. D. Nóbrega, F. C. Fonseca

IPEN-CNEN/SP – 05508-000, São Paulo, SP, Brazil

Carbon resistant and redox stable anodes have been intensively studied aiming at effective fuel-flex solid oxide fuel cells. Previous studies have demonstrated that $La_{0.75}Sr_{0.25}Cr_{0.50}Mn_{0.50}O_3$ (LSCM) perovskite has comparable performance in both hydrogen and methane fueled SOFCs. In the present study, LSCM compounds with partial substitutions of either Mn or Cr by Ru (LSCM-Ru) were synthesized and characterized. Thermal analysis and X-ray diffraction were used to study the thermal evolution of precursor resins and phase formation. The electrical properties were investigated by 4-probe measurements in the 25-800°C temperature range. X-ray diffraction data evidenced that single phase compounds were obtained at 1200°C, without significant structural distortions up to ~ 10 at.% Ru. The electrical resistivity data showed that the transport properties depend on the substituted cation. In addition, the formation of Ru nanoparticles on the surface of LSCM-Ru grains suggests that LSCM-Ru compounds have enhanced catalytic activity for carbon containing fuels.

Introduction

A major goal for research on solid oxide fuel cells (SOFCs) is to have stable operation and high performance using fuels containing carbon. The ceramic-metal composite (cermet) Ni/yttria-stabilized zirconia (Ni/YSZ), the most common material used as the anode of SOFCs, exhibits low tolerance to oxidation-reduction cycles, contaminants, and to carbon deposition (1-5). Such limitations have encouraged the search for alternative anode materials. In this context, oxides with perovskite structure ABO_3 doped with transition metals are interesting candidates because their properties can be controlled by chemical substitutions at both sites A and B of the crystal structure, which can result in the required properties for SOFC anodes.

Among proposed materials to replace the cermet Ni/YSZ, the compound $La_{0.75}Sr_{0.25}Cr_{0.5}Mn_{0,5}O_3$ (LSCM) has attracted a great deal of interest. This ceramic anode has good electrochemical activity using hydrogen, comparable to Ni/YSZ (1,2,6), good catalytic activity for reforming reaction (1-4), and it is stable under oxidizing and reducing atmospheres (6). Previous studies have used LSCM in conjunction with metal or ceramic phases such as Pd and ceria, respectively, aiming at improvement of catalytic properties and transport (7).

In this study, synthesis by the polymeric precursor method and characterization of ceramic anode $La_{0.75}Sr_{0.25}Cr_{0.5}Mn_{0.5}O_3$ (LSCM) with partial substitution of Cr(x) or

Mn(y) for ruthenium Ru ($La_{0.75}Sr_{0.25}Cr_{0.5-x}Mn_{0.5-y}Ru_{x,y}O_3$) are presented. The main goal is the fabrication of redox resistant ceramic anodes with enhanced catalytic activity.

Materials and Methods

The polymeric precursor method was used for the synthesis of ceramic anodes $La_{0.75}Sr_{0.25}Cr_{0.5-x}Mn_{0.5-y}Ru_{x,y}O_3$, where x, y = 0, 0.05, 0.10, and 0.20. In this paper, the compounds are represented by LSC(x%)M(y%)-Ru; for example, x(Cr) = 0.20 is referred as LSC20M-Ru, and y(Mn) = 0.05 as LSCM5-Ru.

The starting metallic salts used were lanthanum nitrate hexahydrate (99.99%), strontium nitrate (> 99%), manganese acetate tetrahydrate (> 99%), chromium nitrate nonahydrate (99%), and ruthenium III chloride hydrate, all from Sigma-Aldrich. The amounts of citric acid (CA) and the volume of ethylene glycol (EG) followed a ratio 60:40 (CA: EG) by weight, and molar ratio between CA and the metal ions was 3:1. Initially, citric acid, ruthenium chloride and distilled water were mixed at ~ 70°C under constant agitation. After ~15 minutes, the remaining cations were added under the same conditions of temperature and agitation, followed by the addition of EG. The mixture was evaporated to obtain a sticky resin that was pre-calcined at 300°C for 1 hour, followed by calcination at 800°C for 5 hours. The obtained powders were heat treated in the 1000-1400°C temperature range in air, and cylindrical pellets were sintered at 1400°C.

The thermal decomposition of polymeric precursor resins was studied by simultaneous thermogravimetry and differential thermal analysis (TG/DTA), Labsys - Setaram, up to 1000°C with a heating rate of 10°C.min^{-1} under synthetic air flow. Phase characterization was carried out by X-ray diffraction (XRD) in the range 20°-90° 2θ range, with step of 0.05° (2θ) and counting time of 2 s, using Cu Kα radiation in a Rigaku Desktop Miniflex diffractometer. The morphology of LSCM-Ru powders heat treated at 1400°C was analyzed by scanning electron microscopy (SEM) and by transmission electron microscopy (JEOL JEM 2100).

Electrical resistance measurements were performed by 4-probe using a Lakeshore 370 resistance bridge, and a digital multimeter (Keithley 2000) monitored the temperature measured by a type K thermocouple positioned close to the sample. Bar samples, cut from cylindrical pellets, with Ag contact pads cured at 600°C, were measured in air from room temperature up to 800°C during heating and cooling (3°C.min^{-1}).

Results and Discussion

The thermal behavior of the resin LSC20M-Ru was analyzed by TG/DTA, as shown in Figure 1. The thermal analyses data revealed that LSCM-Ru compounds have similar thermal behavior and that the addition of ruthenium had no significant effect on the thermal characteristics of the LSCM precursor resin. The total mass loss up to 1000°C was ~60% and occurred in three main steps: at ~90ºC, related to water evaporation, ~250°C, possibly related to the elimination of excess of AC, and the most pronounced mass loss (~45%) in the ~250-500°C range, related to the elimination of organic matter. Above ~600 no significant mass loss was observed. In the DTA curve, peaks associated

with mass loss events were observed, and an exothermic peak without a correspondent mass loss at ~630°C, is possibly related to the crystallization of the oxide phase.

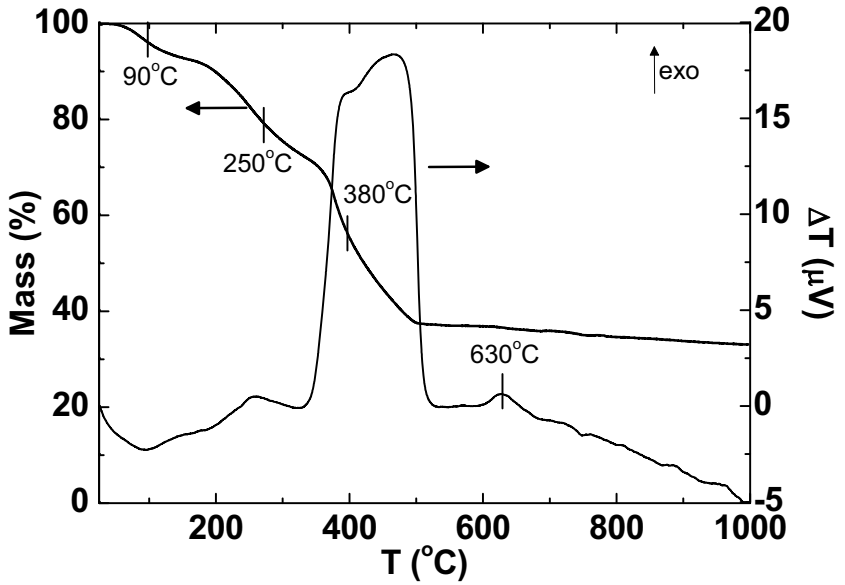

Figure 1. Thermogravimetric curve (left axis) and differential thermal analysis (right axis) of LSC20M-Ru.

The phase formation was investigated by XRD analysis of samples heat treated at different temperatures. Figure 2 shows the evolution of XRD patterns of compounds LSCM, LSC20M-Ru, and LSCM20-Ru heat treated at 800ºC, 1000ºC, 1200ºC and 1400°C for 2 hours. X-ray diffractograms showed that resins treated at 800°C have good crystallinity and all the diffraction peaks corresponding to the LSCM phase. The LSCM-Ru compounds have perovskite structure with rhombohedric crystal system belonging to the $R\bar{3}c$ space group, in agreement with the previous studies (8). However, additional peaks in the 2θ region between ~24° and 30°, probably associated with $SrCrO_4$, indicated that the reactions were not completed at 800°C. With increasing temperature, the peaks of intermediate phases progressively decreased and single phase compounds were obtained after heat treatment at 1200°C. Figure 3 shows the XRD patterns of the two series of LSCM-Ru compounds after sintering at 1400°C.

The X-ray diffractograms of the two series of compounds treated at 1400°C showed only the peaks corresponding to the LSCM, no additional peaks associated with secondary phases were detected. The substitution of Cr or Mn by Ru had a weak effect on the positions of the diffraction peaks up to x, y = 0.10. Increasing the fraction of Ru to x, y = 0.20, results in a shift of the peak position to lower 2θ and a more convoluted doublet at 2θ ~ 33°, the highest relative intensity peak of the LSCM phase. Such features indicated effective substitution of Cr and Mn by Ru in the LSCM crystalline structure. Figure 4 shows the dependence of the lattice parameters $a = b$ and c on the Ru fraction for both series of compounds (LSCxM-Ru and LSCMy-Ru). The calculated lattice parameters were in good agreement with the previously reported data (8) and are weakly dependent on the Ru concentration up to x, y = 0.10. Such s feature is consistent with the similar ionic radii of six-coordinated $Cr^{+3,+4}$, $Mn^{+3,+4}$, and $Ru^{+3,+4}$ (9). However, Ru has a slightly higher ionic radius that is consistent with the increased c parameter observed for the x, y = 0.20 compounds.

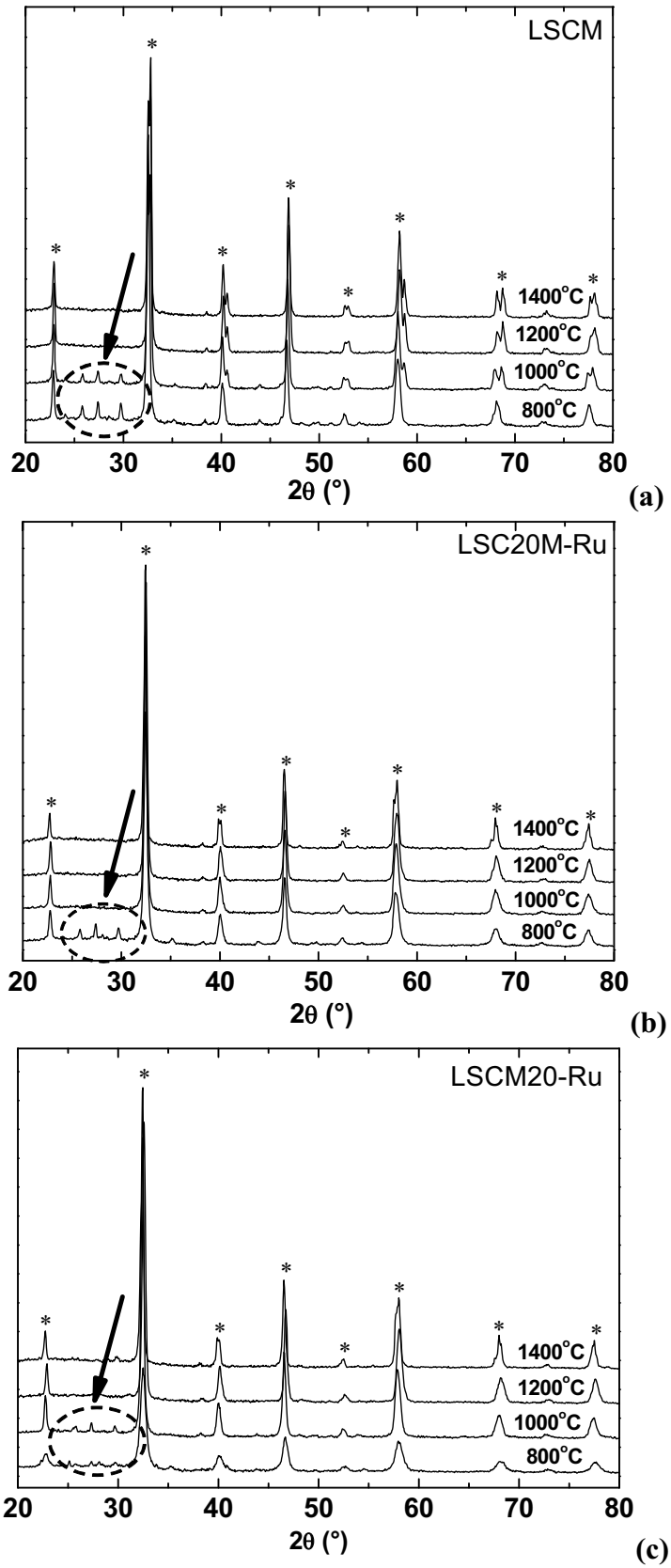

Figure 2. X-ray diffraction patterns of LSCM (a), LSC20M-Ru (b), and LSCM20-Ru (c) heat treated at 800, 1000, 1200 and 1400°C. The symbols (*) mark the indexed diffraction peaks of the compound LSCM (8) and the arrows indicate peaks of intermediate phases.

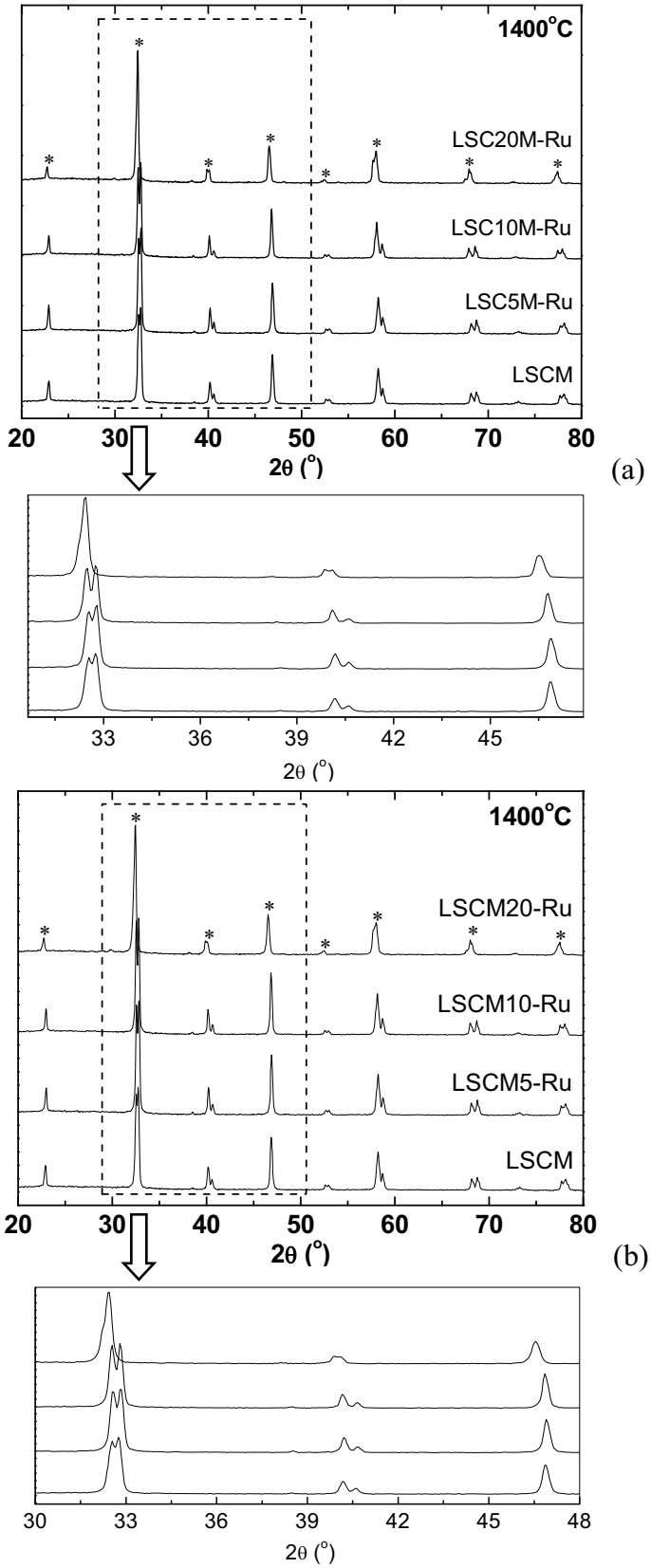

Figure 3. X-ray diffraction patterns of the series (a) LSCxM-Ru and (b) LSCMy-Ru after heat treatment at 1400°C. The symbols (*) mark the indexed peaks of the compound LSCM (8). The arrows indicate the expanded 2θ region of the maximum relative intensity peak.

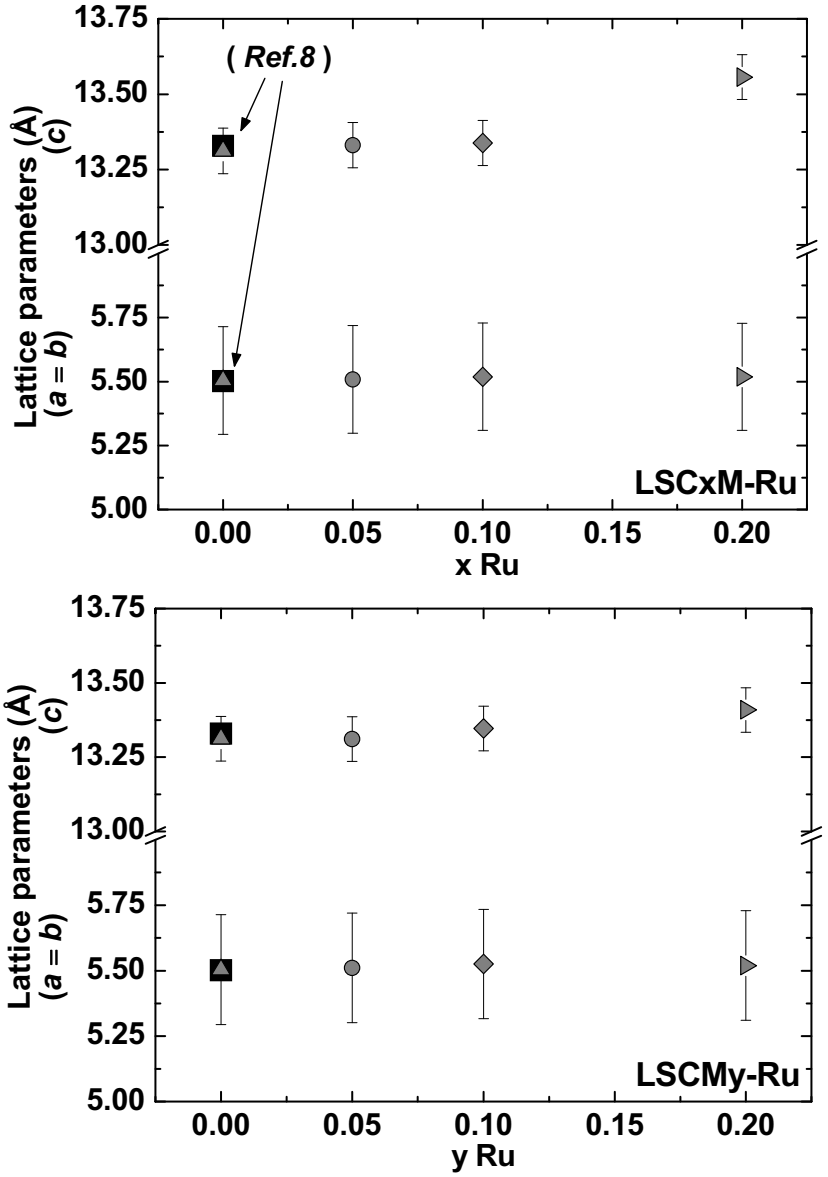

Figure 4. Calculated lattice parameters of $La_{0.75}Sr_{0.25}Cr_{0.5-x}Mn_{0.5-y}Ru_{x,y}O_3$.

Figure 5 shows SEM micrographs of LSC10M-Ru (Fig. 5a and Fig. 5b) and LSCM10-Ru (Fig. 5c and Fig. 5d) powders heat treated at 1400ºC. Powders of LSCM-Ru heat treated at 1400°C exhibit homogeneous distribution of particle sizes, with facetted grains with estimated average size < 1 μm.

The electrical properties of two series of LSCM-Ru compounds were studied in a wide temperature range. The Arrhenius plots are shown in Fig. 6. The LSCM-Ru compounds exhibited thermally activated behavior and electrical conductivity values close to previously reported data (10,11). The electrical conductivity follows the mechanism of adiabatic polaron hopping in a wide temperature range (10). The addition of ruthenium did not alter the transport mechanism of the LSCM, as indicated by calculated values of activation energy (Ea ~0,23 eV). Values of Ea ~0,23 eV are in agreement with the ones previously obtained for LSCM and are practically unchanged upon Ru addition (1,10).

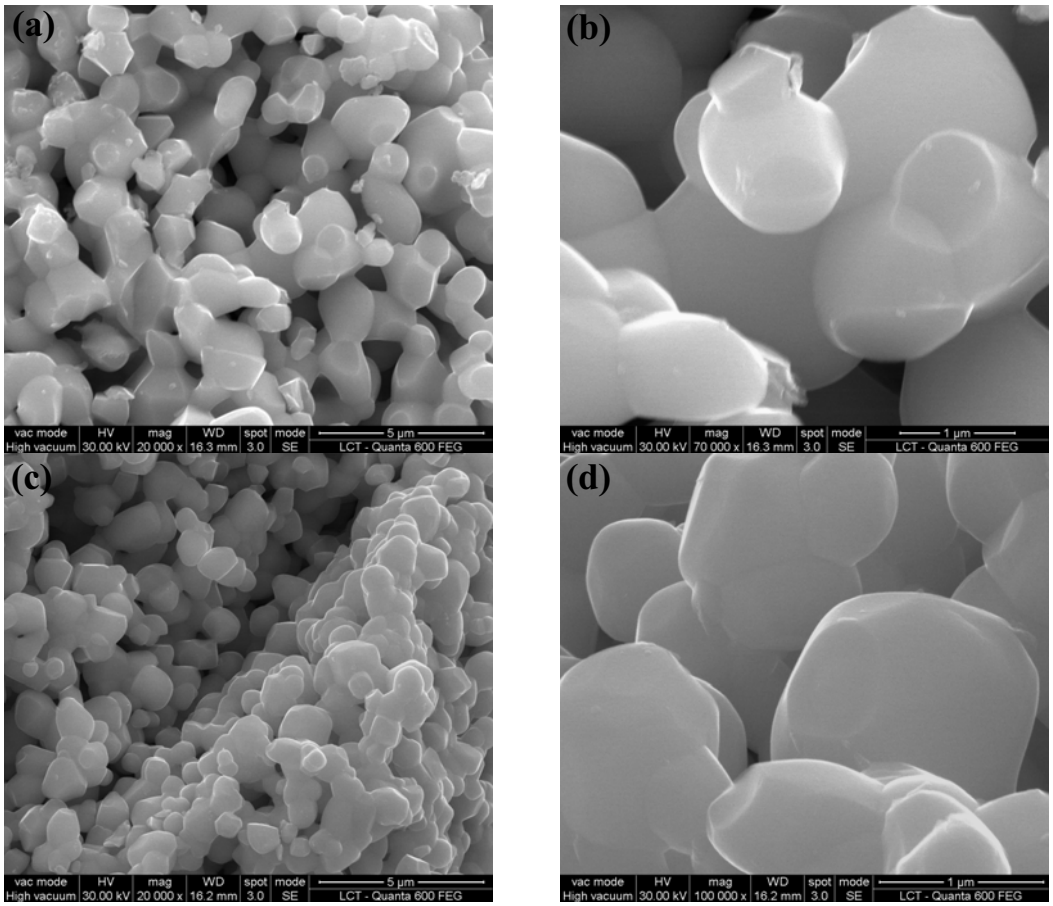

Figure 5. Scanning electron micrographs of LSC10M-Ru (a, b) and LSCM10-Ru (c, d) powders heat treated at 1400°C.

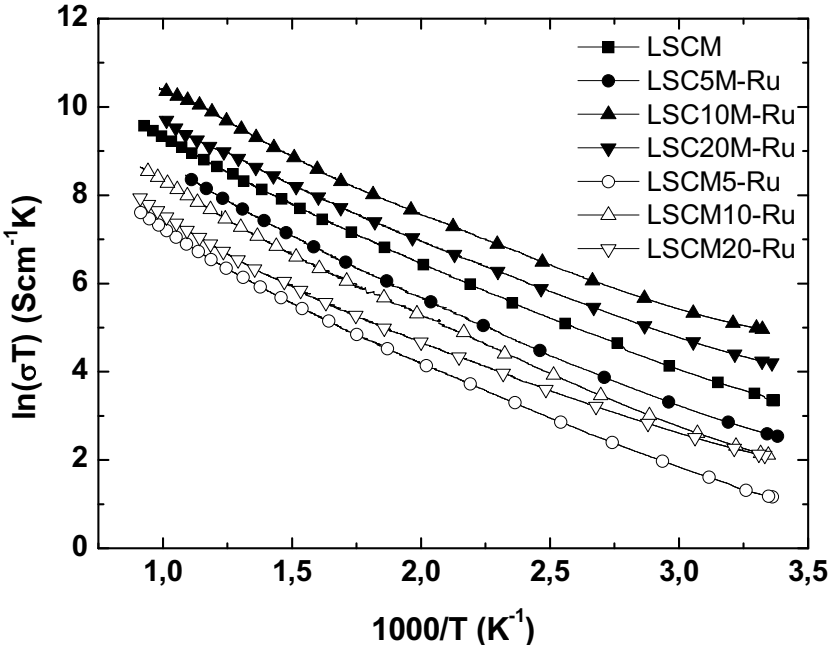

Figure 6. Arrhenius plot of $La_{0.75}Sr_{0.25}Cr_{0.5-x}Mn_{0.5-y}Ru_{x,y}O_3$.

The parent compound LSCM showed intermediate values of electrical conductivity (σ) in comparison to the substituted compounds. The highest values of σ were observed

for the LSC10M-Ru, i.e., x = 0.10 Ru replacing Cr. In general, the substitutions of Cr by Ru resulted in higher values of the electrical conductivity in relation to the LSCM and, conversely, when Mn was substituted by Ru, σ values were approximately one order of magnitude smaller. It was previously determined for LSCM that the average ionic radius of Cr^{+3}/Cr^{+4} is larger than for Mn^{+3}/Mn^{+4}, resulting in larger bonds lengths for Cr^{+3}/Cr^{+4} (8). In addition, it was found that Cr^{+3} is the predominant valence state of Cr in LSCM, suggesting that the hopping of charge carriers occurs primarily via the Mn^{+3}/Mn^{+4} bonds (8). These features are consistent with the σ behavior observed in LSCM-Ru compounds depending on the substituted cation (Fig. 6).

The main idea of the addition of ruthenium in the LSCM is to improve the catalytic properties of the ceramic anode. It has been reported that the catalytic properties of similar Ru-doped perovskites $La_{0.8}Sr_{0.2}Cr_{1-x}Ru_xO_{3-\delta}$ are significantly improved due to the exudation of Ru from the crystal structure (12). Such exuded Ru nanoparticles nucleate on the surface of the parent compound and have interesting catalytic properties, such as a homogeneous distribution and limited coalescence at high temperatures, preserving the high surface area necessary for good catalytic activity.

In order to investigate whether Ru exudes from the crystal structure in the LSCM-Ru, heat treatments at 800°C under H_2 flow were carried out. The resulting samples were analyzed in a transmission electron microscope (TEM), as shown in Fig. 7 for the composition LSC20M-Ru. The TEM images revealed spherical crystalline particles with size ~5 nm on the surface of larger particles. The interplanar distances calculated by the Fourier transform further indicated that such nanoparticles correspond to Ru, suggesting that the LSCM-Ru compounds can exhibit enhanced catalytic properties in reducing environments.

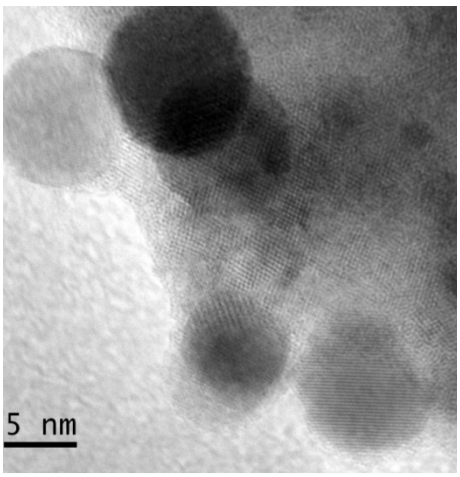

Figure 7. Transmission electron micrograph of the LSC20M-Ru after heat treatment under hydrogen.

Conclusions

$La_{0.75}Sr_{0.25}Cr_{0.50}Mn_{0.50}O_3$ (LSCM) with partial substitution of Mn and Cr by Ru were synthesized. Heat treatment at 1200°C ensured the formation of the desired phase, and Ru substitutions up to 10 at.% had no detectable effect on the crystal structure and the

electrical transport mechanism of the parent compound. The magnitude of the electrical conductivity depends on both the substituted ion and the fraction of Ru, with a maximum magnitude for the composition $La_{0.75}Sr_{0.25}Cr_{0.40}Mn_{0.50}Ru_{0.10}O_3$. Such perovskite can be used to provide stable Ru nanoparticles in reducing conditions, contributing to the catalytic properties of the ceramic anode.

Acknowledgements

This work was partially funded by CNPq, FINEP, and CNEN. The authors thank CNPq for scholarships.

References

1. S. Tao and J.T.S. Irvine, *Nature Materials*, **2**, 5, 320 (2003).
2. Z. Yao, R. Ran and S. Zongping, *Rare Metals*, **28**, 4, 361 (2008).
3. X.C. Lu and J.H. Zhu, *Solid State Ionics*, **178**, 1467 (2007).
4. S.P. Jiang, X.J. Chen, S.H. Chan, J.T. Kwok and K.A. Khor, *Solid State Ionics*, **177**, 149 (2005).
5. X. Zhu, Z. Lü, B. Wei, K. Chen, M. Liu, X. Huang and W. Su, *Journal of Power Sources*, **195**, 1793 (2010).
6. L. Zhang, X. Chen, S.P. Jiang, H.Q. He and Y. Xiang, *Solid State Ionics*, **180**, 1076 (2009).
7. A. Babaei, L. Zhang, S.L. Tan and S.P. Jiang, *Solid State Ionics*, **181**, 1221 (2010).
8. S. Estemirova, A. Fetisov, V. Balakirev and S. Titova, *Journal of Superconductivity and Novel Magnetism*, **20**, 2, 113 (2006).
9. R.D. Shannon, *Acta Crystallographica*, **A32**, 751 (1976).
10. M.P. Ramos, D.Z. Florio and F.C. Fonseca, *Revista Matéria*, **12**, 1, 86 (2006).
11. E. Lay, G. Gauthier, S. Rosini, C. Savaniu and J.T.S. Irvine, *Solid State Ionics*, **179**, 1562 (2008).
12. W. Kobsiriphat, B.D. Madsen, Y. Wang, L.D. Marks and S.A. Barnett, *Solid State Ionics*, **180**, 257 (2009).